Electron beam transport in gas-loaded free-electron lasers

Shalom Yariv and Lazar Friedland
Center for Plasma Physics, Racah Institute of Physics, Hebrew University of Jerusalem, Jerusalem, Israel

(Received 30 January 1990; accepted 27 July 1990)

The effects of the presence of helical wiggler and axial guide magnetic fields on the quality of the electron beam in a gas-loaded free-electron laser are investigated. The electron velocity space diffusion theory in the free-electron laser is developed and tested in Monte Carlo simulations. The theory is applied in estimating the collisional limitations on the interaction length of the laser. It is shown that two competing effects related to collisions cause the gain loss in gas-loaded free-electron lasers, i.e., (a) the growing phase mismatch between the electrons and the wave and (b) the destruction of the coherent transverse helical beam motion. The second effect dominates in the absence of the guide field, provided the wiggler field strength is sufficiently small.

I. INTRODUCTION

Loading a gas into the interaction region of a free-electron laser (FEL) is a very promising method for increasing the laser frequency. This frequency upshift is achieved because the synchronism condition between the wave and the electrons in the laser is modified in the presence of a gas to[1]

$$\lambda \approx \lambda_w \beta_{\mathrm{rel}}, \tag{1}$$

where λ_w is the wiggler period and $\beta_{\mathrm{rel}} = |v/c - 1/n|$ is the absolute value of the relative velocity between the electrons and the wave in the gas in units of the speed of light.

Gas loaded FEL's have attracted a great deal of interest lately[1-3] and a number of investigations, both theoretical[1] and experimental,[2-6] have been published in the last 2 years. In estimating the FEL gain loss due to the scatterings, the Highland velocity spread formula[7] for an *unmagnetized* beam propagating in a gas was employed in all previous studies. In the present work we consider the effects of the presence of a magnetic field on the multiple scattering process in a gas. A wiggler magnetic field is always present in gas-loaded FEL's. We shall also include an axial guide magnetic field in our analysis.

The main difference between an unmagnetized beam transport in a gas and that of a beam in combined wiggler and guide magnetic fields in FEL's is as follows. Small angle elastic scattering of an unmagnetized beam leads to a gradual *decrease* of the average axial velocity of the beam. In the presence of the magnetic fields, characteristic of FEL's, the average velocity of the beam is *fully defined* by the parameters of the fields (steady-state velocity branches[8]). The collisions lead to the *increase* of the *amplitude of oscillations* of perturbations of the steady state. Thus, for example, the average axial velocity of the beam remains *fixed*. We shall develop the theory of the velocity space diffusion of perturbations of these steady states in Sec. II. The diffusion theory will be also tested in Monte-Carlo-type simulations.

Section III is devoted to estimates of the effect of the above-mentioned axial velocity diffusion on the gain and finding the limiting length L_1 of the FEL interaction region for which the effect of the axial velocity spread on the gain is still negligible.

Finally, in Sec. IV, we shall consider another possible mechanism for the gain loss due to collisions, i.e., the destruction of the coherent helical *transverse* motion of the beam. This mechanism yields another limiting laser length L_2. We shall compare the two effects in Sec. IV.

II. VELOCITY SPACE DIFFUSION

Electron beam dynamics in vacuum in combined wiggler and guide magnetic fields has been thoroughly investigated in the past.[8-13] We shall adopt the notations of Ref. 8 and limit our analysis to the vicinity of the wiggler axis, where the normalized cyclotron frequency vector $\mathbf{\Omega} = e\mathbf{B}/mc^2$ associated with the total magnetic field can be written as

$$\mathbf{\Omega} = \Omega \mathbf{e}_z - k_w \xi (\mathbf{e}_x \cos k_w z + \mathbf{e}_y \sin k_w z), \tag{2}$$

where $\Omega = eB_0/mc^2$ describes the axial guide field B_0, while $k_w\xi$ is the cyclotron frequency associated with the *amplitude* of the wiggler fields and $k_w = 2\pi/\lambda_w$. We introduce the following rotating base vectors:

$$\begin{aligned} \mathbf{e}_1 &= \mathbf{e}_x \sin k_w z + \mathbf{e}_y \cos k_w z, \\ \mathbf{e}_2 &= \mathbf{e}_x \cos k_w z - \mathbf{e}_y \sin k_w z, \\ \mathbf{e}_3 &= \mathbf{e}_z, \end{aligned} \tag{3}$$

for which the momentum equation becomes in components[8]

$$\begin{aligned} \dot{u}_1 &= u_2 [k_w u_3 - (\Omega/\gamma)] - (k_w \xi/\gamma) u_3, \\ \dot{u}_2 &= -u_1 [k_w u_3 - (\Omega/\gamma)] \\ \dot{u}_3 &= (k_w \xi/\gamma) u_1, \end{aligned} \tag{4}$$

where $\mathbf{u} = \mathbf{v}/c$, $(\cdots)^{\cdot} = d/d\tau(\cdots)$, and $\tau = ct$.

The steady-state solution of (4) is

$$\begin{aligned} u_1 &= u_{10} = 0, \quad u_3 = u_{30} = \text{const}, \\ u_2 &= u_{20} = \frac{k_w \xi u_{30}/\gamma}{k_w u_{30} - \Omega/\gamma}, \end{aligned} \tag{5}$$

where

$$1/\gamma^2 = 1 - u_{20}^2 - u_{30}^2. \tag{6}$$

There may be more than one set of u_{20} and u_{30} which satisfy (5) and (6).[8]

 0899-8221/90/123114-06$02.00

Near a steady-state solution the electron's velocity components have the following time dependence:[8]

$$u_i = u_{i0} + w_i(\tau), \tag{7}$$

where

$$\begin{aligned} w_1(\tau) &= w_{10}\sin(\mu\tau+\phi), \\ w_2(\tau) &= (a/\mu)w_{10}\cos(\mu\tau+\phi), \\ w_3(\tau) &= -(c/\mu)w_{10}\cos(\mu\tau+\phi), \end{aligned} \tag{8}$$

$$a = \frac{k_w\xi}{\gamma}\frac{u_{30}}{u_{20}}, \quad b = \frac{\Omega}{\gamma}\frac{u_{20}}{u_{30}}, \quad c = \frac{k_w\xi}{\gamma}, \tag{9}$$

and

$$\mu = (a^2 - bc)^{1/2} \tag{10}$$

is the *natural response frequency* of the beam to perturbations. It is also important that an adiabatic change in any of the parameters ξ and Ω will not alter a steady-state solution.[8] For example, suppose that an electron is at some time very close to a steady state (i.e., w_i is very small). An adiabatic change in the above parameters will slowly alter the steady-state velocity so that Eqs. (5) are always satisfied. We demonstrate this adiabatic following of the steady state in Fig. 1, which shows the numerical solution of Eqs. (4) for an electron passing an adiabatic transition region at the entrance into the wiggler with uniform region parameters $\Omega = 2\ \mathrm{cm}^{-1}$, $\xi = 0.3$, $\gamma = 4$, $k_w = 2\ \mathrm{cm}^{-1}$. We see in Fig. 1 the gradual entrance into the steady state with a small perturbation oscillating with the natural response frequency μ. These oscillations grow in time in the presence of collisions, as will be shown later in this section. By defining $x = u_{30}\gamma$, we can combine Eqs. (5) and (6) and obtain the following expression for γ:

$$\gamma = \{1 + x^2[1 + \xi^2/(x - \Omega/k_w)^2]\}^{1/2}, \tag{11}$$

which enables us to plot a graph of $u_{30}(\gamma)$ (see Fig. 2). We distinguish between three branches 1, 2, and 3 as shown in Fig. 2 and note that branch 2 is unstable[8] and thus inapplicable in FEL's.

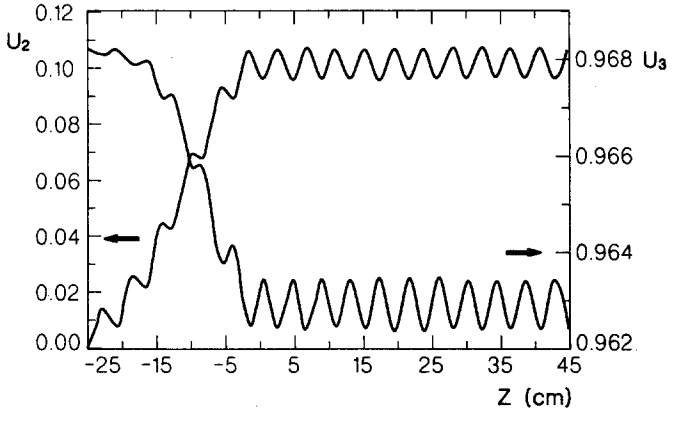

FIG. 1. Axial dependence of the electron velocity components u_2 and u_3 in a wiggler with an adiabatic field increase at the entrance. The example corresponds to the axial beam injection into the wiggler with $\gamma = 4$, $\Omega = 2\ \mathrm{cm}^{-1}$, $k_w = 2\ \mathrm{cm}^{-1}$, and the uniform region value $\xi = 0.3$. The steady-state velocities in this case are $u_{20} = 0.015$ and $u_{30} = 0.968$.

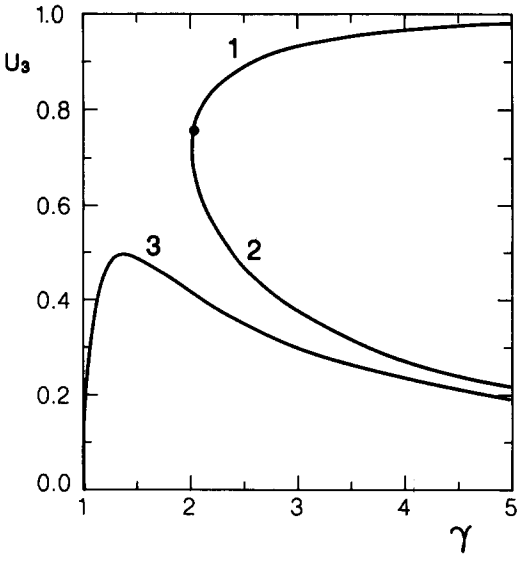

FIG. 2. The steady-state solution u_{30} versus the relativistic factor γ for $\Omega/k_w = 1.0$ and $\xi = 0.3$. The three solution branches are shown by the numbers (1,2,3).

At this point, being interested in the evolution of perturbations w_i [see Eq. (8)], we observe that the projections of the solution $\mathbf{u} = \mathbf{u}_0 + \mathbf{w}(\tau)$ on the two-dimensional velocity subspaces (u_1,u_2) and (u_1,u_3) form ellipses, each with a period $T = 2\pi/\mu$. Indeed [see Eq. (8)]

$$\begin{aligned} w_1^2 + (\mu/a)^2 w_2^2 &= w_{10}^2, \\ w_1^2 + (\mu/c)^2 w_3^2 &= w_{10}^2. \end{aligned} \tag{12}$$

These two ellipses turn out to be different projections of a single ellipse. The following coordinate transformation leads to a base in which two coordinate axes are along the axes of this ellipse, and the third is perpendicular to its plane:

$$\begin{aligned} \lambda_1 &= w_1, \\ \lambda_2 &= w_2\cos\theta + w_3\sin\theta, \\ \lambda_3 &= w_2\sin\theta - w_3\cos\theta, \end{aligned} \tag{13}$$

where $\tan\theta = c/a$. Now we see that always $\lambda_3 = 0$, $\lambda_2 = (w_2^2 + w_3^2)^{1/2}$, and in the (λ_1,λ_2) plane the electron trajectory satisfies

$$\lambda_1^2 + [\mu^2/(a^2 + c^2)]\lambda_2^2 = w_{10}^2, \tag{14}$$

i.e., the equation of an ellipse. The geometry of the transformation is shown in Fig. 3. Since the steady-state velocity vector $\mathbf{u}_0$ is not affected by elastic collisions, a single angular elastic scattering process can be viewed within our model (accurate to first order in w_i) as an instantaneous displacement in the (λ_1,λ_2) plane from a vector $\boldsymbol{\lambda} = (\lambda_1,\lambda_2)$ to another vector

$$\boldsymbol{\lambda}' = (\lambda_1',\lambda_2') = (\lambda_1,\lambda_2) + (\rho_1,\rho_2), \tag{15}$$

where

$$\rho_1 = \rho\cos\alpha, \quad \rho_2 = \rho\sin\alpha, \tag{16}$$

α being the azimuthal scattering angle, and

$$\rho = |\mathbf{u}|\sin\Theta \approx \Theta, \tag{17}$$

where Θ is the scattering angle with respect to the direction

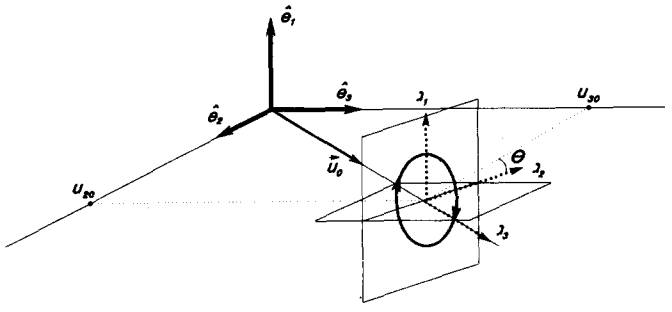

FIG. 3. Geometry of the transformation to $(\lambda_1,\lambda_2,\lambda_3)$ coordinates. The electron trajectory lies in the (λ_1,λ_2) plane.

of $\mathbf{u}$ before the scattering. For the two vectors $\boldsymbol{\lambda}$ and $\boldsymbol{\lambda}'$ before and after the scattering, we have [see Eq. (14)]

$$\lambda_1^2 + [\mu^2/(a^2+c^2)]\lambda_2^2 = w_{10}^2 \tag{18}$$

and

$$\lambda_1'^2 + [\mu^2/(a^2+c^2)]\lambda_2'^2 = w_{10}'^2. \tag{19}$$

Equations (15)–(19) then yield the following relation between w_{10}' and w_{10}:

$$w_{10}'^2 = w_{10}^2 + 2\rho\{\lambda_1 \cos\alpha + [\mu^2/(a^2+c^2)]\lambda_2 \sin\alpha\} + \rho^2\{\cos^2\alpha + [\mu^2/(a^2+c^2)]\sin^2\alpha\}. \tag{20}$$

At this stage we average over the azimuthal scattering angle α, and assume that ρ is independent of α. This yields

$$\langle w_{10}'^2\rangle = \langle w_{10}^2\rangle + \tfrac{1}{2}\langle\rho^2\rangle\{1 + [\mu^2/(a^2+c^2)]\}. \tag{21}$$

Thus after N scatterings we obtain

$$\langle w_{10}'^2(N)\rangle = w_{10}^2(0) + D_1 N, \tag{22}$$

where

$$D_1 = \tfrac{1}{2}\langle\rho^2\rangle\{1 + [\mu^2/(a^2+c^2)]\} \tag{23}$$

is the effective velocity space diffusion coefficient.

By using the fact that w_{20} and w_{30} are linearly related to w_{10}, we obtain

$$\langle w_{20}'^2(N)\rangle = w_{20}^2(0) + D_2 N, \tag{24}$$

$$\langle w_{30}'^2(N)\rangle = w_{30}^2(0) + D_3 N, \tag{25}$$

where

$$D_2 = \frac{1}{2}\langle\rho^2\rangle\left(\frac{a^2}{\mu^2} + \frac{a^2}{a^2+c^2}\right) \tag{26}$$

and

$$D_3 = \frac{1}{2}\langle\rho^2\rangle\left(\frac{c^2}{\mu^2} + \frac{c^2}{a^2+c^2}\right). \tag{27}$$

The dependence of D_3 on Ω and ξ is given in Fig. 4 for two stable steady branches 1 and 3 (see Fig. 2). We observe that D_3 is always smaller on branch 3 than on branch 1. This fact is important since the growth of $\langle w_{30}^2\rangle$ in collisions is one of the factors responsible for the gain loss in the FEL, as will be shown in the next section.

In order to check our theory, we performed calculations including Monte-Carlo-type simulations of small angle scat-

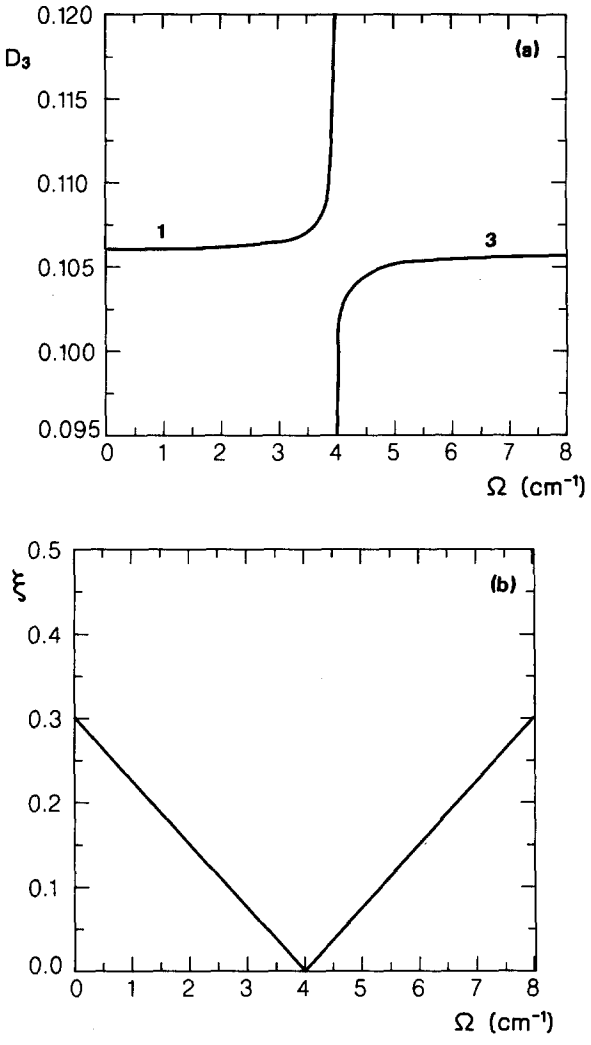

FIG. 4. The results of the velocity-space diffusion theory in combined wiggler and guide magnetic fields for stable branches 1 and 3. (a) The diffusion coefficient D_3 vs Ω. (b) The dependence of the wiggler parameter ξ on Ω used in evaluating D_3 in (a) in order to preserve the value of u_{20} for a given wiggler pitch and electron energy ($k_w = 1\ \mathrm{cm}^{-1}$ and $\gamma = 4$).

terings along the electron trajectories in the FEL. Electron motion between the collisions in this calculation was found by numerically solving the exact momentum equations (4). The random normalized time interval between the collisions was modeled according to $\Delta\tau = -(\lambda_{\mathrm{coll}}/u)\ln\eta$, where $u = |\mathbf{u}| = (1 - 1/\gamma^2)^{1/2}$, λ_{coll} was the mean-free path, and η were computer-generated pseudorandom numbers distributed uniformly in the interval [0,1]. Each elastic scattering was assumed to be azimuthally isotropic and the azimuthal scattering angle α was chosen randomly between 0 and 2π by again using the random numbers η generated by the computer. The small scattering angle Θ, relative to the direction of the velocity $\mathbf{u}$ before the scattering, was taken to be a constant Θ_0, for simplicity. Figure 5 shows a typical electron trajectory in the (u_1,u_2) plane and the corresponding dependence of u_3 on z. The parameters in the figure are $\gamma = 10.1$, $\Omega = 15\ \mathrm{cm}^{-1}$, $k_w = 1\ \mathrm{cm}^{-1}$, $\xi = 0.5$, $\Theta_0 = 10^{-3}$, and $\lambda_{\mathrm{coll}} = 0.12$ cm. Figure 6 illustrates the good agreement

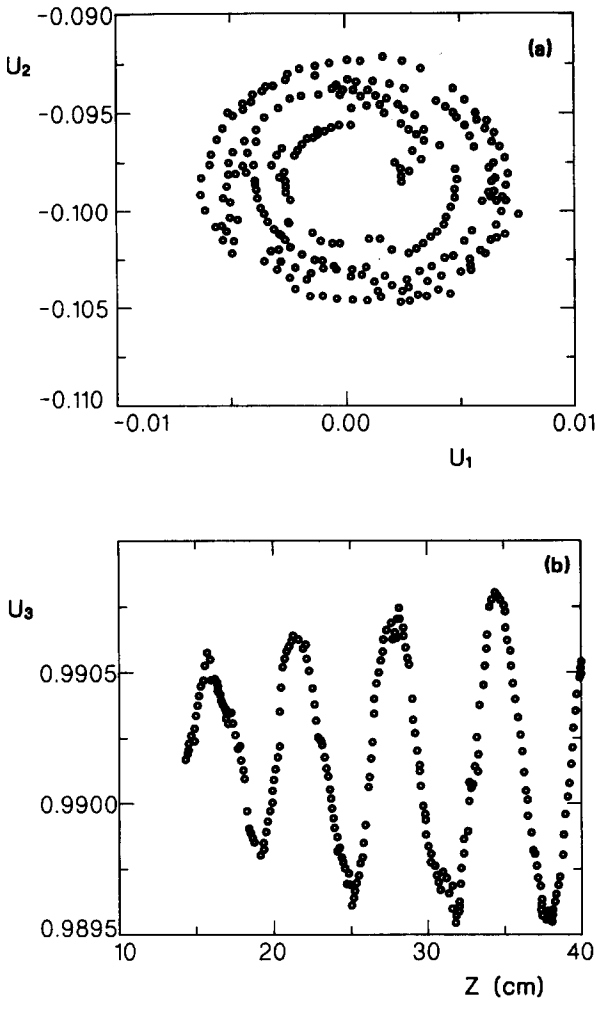

FIG. 5. Typical computer simulations of the electron motion in a gas in combined wiggler and guide magnetic fields. (a) A typical electron trajectory in the (u_1,u_2) plane. The parameters are $\gamma = 10.1$, $\Omega = 15\ \mathrm{cm}^{-1}$, $k_w = 1\ \mathrm{cm}^{-1}$, $\xi = 0.5$, $\Theta_0 = 10^{-3}$, and $\lambda_{\mathrm{coll}} = 0.12$ cm. Between the collisions the particle moves on eccentric ellipses, with random jumps between the ellipses due to the collisions. (b) The z dependence of u_3, corresponding to the simulations shown in (a).

between our diffusion theory and the simulations for several wiggler and beam parameters. The averages were found by performing the simulations for the total of 250 test electrons for each case in the figure.

III. GAIN LOSS IN A GAS DUE TO THE AXIAL PHASE MISMATCH

The small signal gain in free-electron lasers is critically dependent on the phase $\psi = (k + k_w)z - \omega t$ where the wiggling electrons see the electromagnetic wave. For an appreciable gain, one requires that the phase mismatch between individual electrons due to such factors as energy spread, velocity spread in collisions, etc., satisfy the condition

$$\Delta|\psi| < \pi. \tag{28}$$

Then by using

$$z = u_{30}t + \int_0^t w_3(t')dt' \tag{29}$$

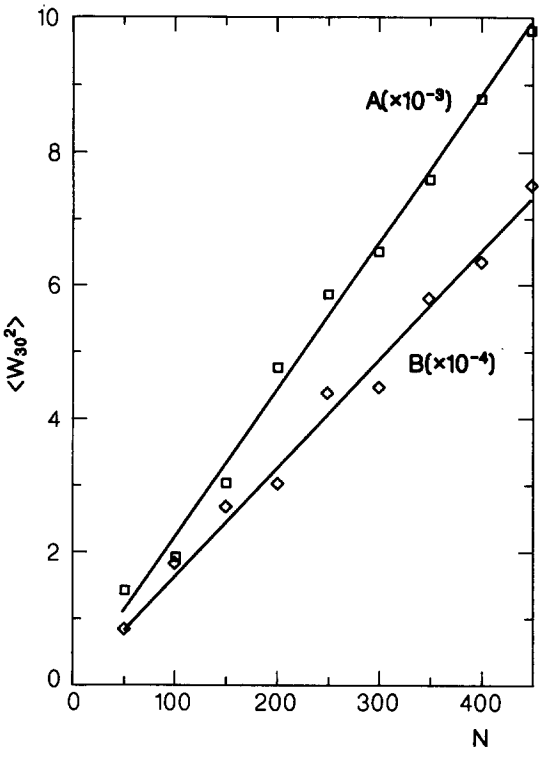

FIG. 6. The comparison of the diffusion theory for $\langle w_{30}^2 \rangle$ (solid line) with the simulations (dots). Case A: $\gamma = 1.5$, $\Omega = 1\ \mathrm{cm}^{-1}$, $k_w = 1\ \mathrm{cm}^{-1}$, $\xi = 1.0$, and $\Theta_0 = 0.01/\gamma$ $(D_3 = 2.2\times10^{-5})$; case B: $\gamma = 2.29$ $(D_3 = 1.63\times10^{-6})$.

and requiring full phase matching in the steady state, i.e., $(k + k_w)u_{30} - \omega = 0$, we can rewrite (28) as

$$S = \Delta\left(\int_0^t w_3(t')dt'\right) < \frac{\pi}{k + k_w}. \tag{30}$$

At this point we shall estimate the left-hand side of (30) by using the diffusion theory of Sec. II. Since the growth of S here is associated with collisions, we shall use the rms value for S in our estimates, i.e.,

$$S = \left|\left\langle\left(\int_0^t w_3(t')dt'\right)^2\right\rangle - \left\langle\int_0^t w_3(t')dt'\right\rangle^2\right|^{1/2}. \tag{31}$$

Between successive collisions (say k and $k+1$) here we can substitute [see Eq. (8)]

$$w_3^k(t') = w_{30}^k \cos(\mu t' + \varphi^k), \quad t_k \leqslant t' < t_{k+1};\ k = 1,2,\ldots,N, \tag{32}$$

where t_k is the time moment of the k th collision. It is convenient now to transform to the variables λ_i defined earlier [see Eq. (13)]. Since $w_3 = c\lambda_2/(a^2 + c^2)^{1/2}$, we have

$$w_3^k(t) = [c\lambda_{20}^k/(a^2 + c^2)^{1/2}]\cos(\mu t + \varphi^k). \tag{33}$$

The use of the new variables λ_i is advantageous here because the azimuthal scattering is isotropic in this coordinate system (see Fig. 3).

Now, the two terms in the right-hand side of (31) become

$$I_1=\frac{c^2}{\mu^2(a^2+c^2)}\left\langle\sum_{k=0}^{N}\lambda_{20}^{k}\left[\sin(\mu t_{k+1}+\varphi^k)-\sin(\mu t_k+\varphi^k)\right]\right\rangle^2 \tag{34}$$

and

$$I_2=\frac{c^2}{\mu^2(a^2+c^2)}\left\langle\left(\sum_{k=0}^{N}\lambda_{20}^{k}\left[\sin(\mu t_{k+1}+\varphi^k)-\sin(\mu t_k+\varphi^k)\right]\right)\right\rangle^2. \tag{35}$$

Starting from I_1, we rewrite it as

$$I_1=\frac{c^2}{\mu^2(a^2+c^2)}\left(\langle\lambda_{20}^{0}\sin(\mu t_0+\varphi^0)\rangle+\left\langle\sum_{k=1}^{N}\left[\lambda_{20}^{k}\sin(\mu t_k+\varphi^k)-\lambda_{20}^{k-1}\sin(\mu t_k+\varphi^{k-1})\right]\right\rangle-\langle\lambda_{20}^{N}\sin(\mu t_{N+1}+\varphi^N)\rangle\right)^2. \tag{36}$$

The first and the last terms in the sum in (36) vanish because of the random values of φ^0 (the initial phase) and φ^N. Furthermore, $\lambda_{20}^{k}\sin(\mu t_k+\varphi^k)$ equals $\lambda_{20}\lambda_1/\lambda_{10}$ immediately after the k th collision, while $\lambda_{20}^{k}\sin(\mu t_k+\varphi^{k-1})$ equals $\lambda_{20}\lambda_1/\lambda_{10}$ just before the k th collision. Thus

$$\lambda_{20}^{k}\sin(\mu t_k+\varphi^k)-\lambda_{20}^{k-1}\sin(\mu t_k+\varphi^{k-1})=\rho\sin\alpha_k, \tag{37}$$

and the averaging over α_k yields

$$I_1=\frac{c^2}{\mu^2(a^2+c^2)}\left\langle\rho\sum\sin\alpha_k\right\rangle^2=0. \tag{38}$$

Similarly,

$$I_2=\frac{c^2}{\mu^2(a^2+c^2)}\left[\left\langle\left(\sum_{k=1}^{N}\rho\sin\alpha_k\right)\right\rangle^2+\langle[\lambda_{20}^{N}\sin(\mu t_{N+1}+\varphi^N)]^2\rangle\right]=\frac{c^2}{\mu^2(a^2+c^2)}\left(\frac{\rho^2}{2}N+\frac{1}{2}\langle(\lambda_{20}^{N})^2\rangle\right). \tag{39}$$

From the diffusion theory [see Eqs. (12), (14), and (25)] we have

$$\langle(\lambda_{20}^{N})^2\rangle=[(a^2+c^2)/c^2]\langle(w_{30}^{N})^2\rangle=D_{\lambda_2}N, \tag{40}$$

with

$$D_{\lambda_2}=\tfrac{1}{2}\rho^2[1+(a^2+c^2)/\mu^2]. \tag{41}$$

Thus, finally [see Eq. (31)]

$$S=\sqrt{N}\,\Theta, \tag{42}$$

where

$$\Theta\equiv\frac{\rho}{\sqrt{2\mu}}\left[\left(\frac{3}{2}+\frac{1}{2}\frac{a^2+c^2}{\mu^2}\right)\right]^{1/2}\frac{c}{(a^2+c^2)^{1/2}}. \tag{43}$$

The average number N of collisions in the wiggler is

$$N=L/\lambda_{\rm coll}, \tag{44}$$

where $\lambda_{\rm coll}$ is the mean-free path for elastic collisions, and L is the length of the wiggler. Then inequality (30) yields an estimate for the maximum allowed length of the wiggler L_1 for which the small signal gain is only weakly affected by the growing mismatch between the electrons and the wave:

$$L_1\cong\lambda_{\rm coll}[\pi/(k+k_w)\Theta]^2. \tag{45}$$

IV. COLLISIONAL LOSS OF COHERENT TRANSVERSE BEAM MOTION

All conventional theories calculate the small signal gain in an FEL by assuming a weak perturbation of the helical steady state. This coherency assumption is obviously violated once the condition $w_{20}\ll u_{20}$ does not hold. Collisions can lead to the violation of this condition. Let us consider this effect. Equations (24) and (26) yield

$$w_{20}^2(N)=w_{20}^2(0)+\frac{N}{2}\left(1+\frac{\mu^2}{a^2+c^2}\right)\frac{a^2}{c^2}. \tag{46}$$

By again using $N=L/\lambda_{\rm coll}$ and assuming that $w_{20}^2(0)\ll ND_2$, we can now estimate the maximum wiggler length for which the *coherent transverse motion* is still present:

$$L_2=\frac{\lambda_{\rm coll}}{\rho^2}\frac{2\mu^2}{a^2}\frac{u_{20}^2}{[1+\mu^2/(a^2+c^2)]}. \tag{47}$$

By substituting the microscopic quantities $\lambda_{\rm coll}$ and ρ,[14] we can obtain convenient formulas for L_1 [see Eq. (45)] and L_2:

$$L_2\,({\rm cm})=\frac{2400}{P({\rm atm})}\left(\frac{\mu^2}{a^2}\frac{u_{20}^2}{[1+\mu^2/(a^2+c^2)]}\right)\gamma^2,$$

$$L_1\,({\rm cm})=\frac{2400}{P({\rm atm})}\left(\frac{\mu^2}{c^2}\frac{a^2+c^2}{[\frac{3}{2}+\frac{1}{2}(a^2+c^2)/\mu^2]}\times\frac{\pi^2}{(k+k_w)^2}\right)\gamma^2. \tag{48}$$

Clearly, to neglect the gain loss in the FEL due to collisions, we must require that

$$L<\min(L_1,L_2). \tag{49}$$

Figure 7 shows L_1 and L_2 vs Ω, keeping $|u_{20}|$, u_{30}, and γ constant, i.e., holding the laser wavelength fixed. The constancy of these parameters is achieved by changing ξ as Ω is varied. The appropriate relation between ξ and Ω is [see Eq. (5)]

$$\xi(\Omega)=(u_{30}\gamma-\Omega/k_w)(u_{20}/u_{30}). \tag{50}$$

The limiting length L_u of the FEL as given by the unmagnetized beam scattering theory,[1]

$$L_u\,({\rm cm})=28[\gamma\lambda^{1/2}({\rm cm})/P^{1/2}({\rm atm})], \tag{51}$$

is also shown in Fig. 7 for comparison (the dashed line). We see in the figure that there are regions in which different effects limit the laser length. We observe that for $\Omega=0$ the development of the axial phase mismatch limits the length of the interaction region in the example shown in Fig. 7. Also, the unmagnetized beam scattering theory[1] underestimates the limiting laser length for $\Omega=0$ in Fig. 7.

Finally, let us consider two limiting cases in more detail. First, we look at the case of zero guide magnetic field. In this

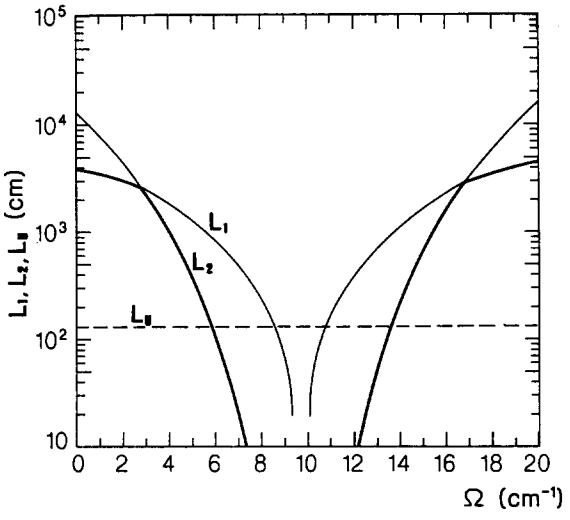

FIG. 7. L_1 and L_2 vs Ω for $\gamma = 10.25$, $k_w = 1\ \mathrm{cm}^{-1}$, $\xi = 2.0$ at $\Omega = 0$, and $P = 1$ atm. Here $L_{\min}$ is represented by a heavy solid line; L_u shows the result of the unmagnetized beam scattering approximation.

case $a = \mu$, $u_{20} = \xi/\gamma$, and $c/a = \xi/u_{30}\gamma$. Let us assume that $\xi \ll \gamma$. Then $u_{30} \approx 1$, $k \approx 2\gamma^2 k_w$, $a \gg c$, and, therefore, we obtain

$$L_2/L_1 \approx 4\xi^2/\pi^2. \tag{52}$$

Thus the loss of the coherent transverse motion due to collisions limits the length of the laser without the guide fields if $\xi < \pi/2$ (unlike the case shown in Fig. 7, where $\xi = 2$).

Now let us consider another extreme, i.e., the case when one approaches the cyclotron resonance $\Omega \to \gamma k_0 u_{30}$. In this case $\xi \to 0$ [see Eq. (41)]. Simple algebra then yields

$$L_2/L_1 \to 1/\xi. \tag{53}$$

Thus the growing mismatch between the wave and the beam is responsible for the gain loss in this limiting case.

Finally, we see in Fig. 7 that with the increase of Ω, when Ω becomes much larger than $k_w u_{30}\gamma$ (this, of course, can only be achieved if γ is not too large), both L_1 and L_2 increase, indicating the possibility of utilizing a longer interaction region for a given gas pressure.

V. CONCLUSIONS

The effects of the presence of the wiggler and the axial guide magnetic fields on the quality of the electron beam in a gas-loaded FEL were investigated in this work.

It was shown that in the presence of the magnetic fields, the velocity space diffusion of the electrons in the beam due to the multiple small angle scatterings in a gas differ significantly from that for an unmagnetized beam. The theory of this diffusion process in an FEL was developed and tested in Monte-Carlo-type simulations.

The diffusion theory was applied in estimating the limiting interaction length in gas-loaded FEL's for which the effect of collisions on the small signal gain is still small.

It was shown that two different collisional effects cause the gain loss in gas-loaded FEL's. The first is the growing mismatch between the phases where the individual electrons in the beam see the electromagnetic wave. The second effect is related to the destruction of the coherent helical transverse motion of the beam due to collisions.

In the zero guide field case the second collisional effect is dominant, provided the cyclotron frequency associated with the wiggler field is less than $\pi c k_w/2$. In contrast, if one operates the laser with the guide field near the cyclotron resonance, the phase mismatch growth in collisions is the dominant gain loss mechanism.

[1] A. M. Fauchet, J. Feinstein, A. Gover, and R. H. Pantell, IEEE J. Quantum Electron. **QE-20**, 1332 (1984).
[2] R. H. Pantell, J. Feinstein, A. S. Fisher, T. L. Deloney, M. B. Reid, and W. M. Grossman, Nucl. Instrum. Methods A **250**, 312 (1986).
[3] J. Feinstein, A. S. Fisher, M. B. Reid, A. Ho, and M. Oezcan, Phys. Rev. Lett. **60**, 1982 (1988).
[4] M. B. Reid and R. Pantell, IEEE J. Quantum Electron. **QE-25**, 84 (1989).
[5] M. B. Reid, A. S. Fisher, J. Feinstein, A. Ho, M. Öszcan, H. D. Dulman, Y. J. Lee, and R. H. Pantell, Phys. Rev. Lett. **62**, 249 (1989).
[6] R. H. Pantell, A. S. Fisher, J. Feinstein, A. H. Ho, M. Özcan, H. D. Dullman, and M. B. Reid, J. Opt. Soc. Am. B **6**, 1008 (1987).
[7] V. L. Highland, Nucl. Instrum Methods **129**, 497 (1975).
[8] L. Friedland, Phys. Fluids **23**, 2376 (1980).
[9] A. S. Fisher, R. H. Pantell, J. Feinstein, T. L. Delony, M. B. Reid, and W. M. Grossman, Nucl. Instrum. Methods A **250**, 337 (1985).
[10] R. C. Davidson and H. S. Uhm, Phys. Fluids **23**, 2076 (1980).
[11] R. C. Davidson and H. S. Uhm, J. Appl. Phys. **53**, 2910 (1982).
[12] H. F. Freund and A. T. Drobot, Phys. Fluids **25**, 736 (1983).
[13] C. Chen and G. Schmidt, Comments Plasma Phys. **12**, 83 (1988).
[14] N. F. Mott and H. S. W. Massey, *The Theory of Atomic Collisions* (Oxford U.P., Oxford, 1965).